Atmos. Chem. Phys. Discuss., 12, 20901–20930, 2012
www.atmos-chem-phys-discuss.net/12/20901/2012/
doi:10.5194/acpd-12-20901-2012

Atmospheric Chemistry and Physics Discussions

A data assimilative perspective of oceanic mesoscale eddy evolution during VOCALS-REx

A. C. Subramanian[1], A. J. Miller[1], B. D. Cornuelle[1], E. Di Lorenzo[2], R. A. Weller[3], and F. Straneo[3]

[1]Scripps Institution of Oceanography, University of California, San Diego, La Jolla, California, USA
[2]Georgia Institute of Technology, Altlanta, Georgia, USA
[3]Woods Hole Oceanographic Institution, MIT, 86 Water Street, MA, USA

Received: 25 July 2012 – Accepted: 6 August 2012 – Published: 20 August 2012

Correspondence to: A. C. Subramanian (acsubram@ucsd.edu)

Published by Copernicus Publications on behalf of the European Geosciences Union.

Abstract

Oceanic observations collected during the VOCALS-REx cruise time period, 1–30 November 2008, are assimilated into a regional ocean model (ROMS) using 4DVAR and then analyzed for their dynamics. Nonlinearities in the system prevent a complete 30-day fit, so two 15-day fits for 1–15 November and 16–30 November are executed using the available observations of hydrographic temperature and salinity, along with satellite fields of SST and sea-level height anomaly. The fits converge and reduce the cost function significantly, and the results indicated that ROMS is able to successfully reproduce both large-scale and smaller-scale features of the flows observed during the 76° W, 19° S. The ROMS fits capture this eddy as an isolated rotating 3-D vortex with a strong subsurface signature in velocity, temperature and anomalously low salinity. The eddy has an average temperature anomaly of approximately −0.5 °C over a depth range from 50–600 m and features a cold anomaly of approximately −1 °C near 150 m depth. The eddy moves northwestward and elongates during the second 15-day fit. It exhibits a strong signature in the Okubo-Weiss parameter, which indicates significant nonlinearity in its evolution. The heat balance for the period of the cruise from the ocean state estimate reveals that the horizontal advection and the vertical mixing processes are the dominant terms that balance the temperature tendency of the upper layer of the ocean locally in time and space. Areal averages, however, around the eddies and around the cruise tracks, suggest that vertical mixing processes generally balance the surface heating, indicating only a small role for lateral advective processes in this region.

1 Introduction

The climate of the Southeast Pacific (SEP) involves important feedbacks between atmospheric circulation, sea-surface temperature (SST), clouds, ocean heat transport, aerosols, coastal orography, bathymetry and geometry (Mechoso et al., 1995; Ma et al.,

ACPD
12, 20901–20930, 2012

1996; Xie, 2004). The Andes mountains channel strong southerly winds along the coast generating vigorous coastal upwelling (Garreaud and Muñoz, 2005; Amador et al., 2006). The resulting equatorward Peru-Humboldt Current is baroclinically unstable and develops nonlinear mesoscale eddies and waves that re-distribute the cold water more than a thousand kilometers offshore (Penven, 2005; Colas et al., 2011). The cool water helps maintain the low-level clouds, whose shade helps keep the waters cool (Klein and Hartmann, 1993; Zheng et al., 2011). The cloud formation depends on aerosols, which are produced both by ocean biology (which is dependent on upwelled, recycled and transported nutrients) and by human industrial activities along the coast (Hind et al., 2011; Yang et al., 2011, 2009).

The VOCALS (VAMOS Ocean Cloud Atmosphere Land Study) REx (Regional Experiment) campaign was designed to address the fundamental dynamics that control the large-scale ocean-atmosphere system in the SEP (Wood et al., 2011; Zheng et al., 2011). Teams of national and international collaborators measured, analyzed, and modeled the large-scale atmospheric subsidence, broad regions of stratocumulus clouds, cool sea-surface temperature, upwelling ocean boundary currents and energetic mesoscale ocean eddies, which all interact in complicated ways to affect local, basin-scale and global-scale climate variability (Mechoso et al., 1995; Wood et al., 2011).

The mesoscale eddies of the ocean circulation observed during VOCALS-REx make up the component of the system that is the focus of this study. These eddies can affect the distribution of sea-surface temperature (SST) in the eastern tropical Pacific in two major ways. The eddy heat fluxes along with vertical mixing processes in the region drive SST changes that affect the atmospheric boundary layer by altering its stability and consequent heat, momentum and moisture fluxes at the air-sea interface (Large and Danabasoglu, 2006; Capet et al., 2008; de Szoeke et al., 2010; Zheng et al., 2010). The eddies also affect nutrient transport to and within the euphotic zone, which controls ocean biology. Chelton et al. (2011) show that on timescales greater than 2–3 weeks, eddy-induced horizontal advection of chlorophyll is the dominant mechanism

ACPD
12, 20901–20930, 2012

that determines the chlorophyll variability in eddy active regions such as the SEP. Eddies consequently affect air-sea fluxes of volatile organic compounds, such as DMS, that convert into cloud condensation nuclei and radiative scattering aerosols in the atmosphere (Clarke, 1998; Albert et al., 2010; Yang et al., 2009, 2011).

In order to better understand the time-dependent evolution of the eddy field that was observed during VOCALS-REx, we use an ocean data assimilation technique to produce a time-dependent reconstruction of the flow fields around the cruise tracks. The resulting "fits" give a more complete depiction of the key ocean eddy components of the system that were studied using observations alone by Holte et al. (2012). By constraining the observations with ocean dynamics, for example, we can follow a key subsurface eddy, and analyze its water mass properties and its dynamics and isolate the upper-ocean heat balance terms during the cruises. We can also quantify the level of nonlinearity in the system and offer a dynamical view about dominant processes that could have influenced the biogeochemical processes during the campaign.

Section 2 describes the data available for the assimilation experiment. Section 3 presents the basics of the model and the assimilation procedure. Section 4 describes the results of fits, and Section 5 provides a summary and discussion of results.

2 Observations during VOCALS-REx

2.1 Oceanographic in-situ data

Subsurface temperature and salinity data were collected by CTD casts along the VOCALS cruise tracks (Wood et al., 2011), which are shown in Fig. 1. At each of the REx major hydrographic stations, marked as large dots, CTD casts to 3500 m (or near the ocean bottom) were taken over the 38 day experimental time period. Additionally, Underway CTD casts were obtained, typically to depths of 500m, while underway between these stations. The measurements span the range of 19° S to 21.5° S and 86° W to 72° W, with a number of stations taken to sample an eddy that was encountered near

ACPD
12, 20901–20930, 2012

20° N, 76° W. A number of Argo floats also sampled the water column during this time period.

2.2 Satellite data

SST data were available from the 10km resolution blended satellite product which combines Japan's Advanced Microwave Scanning Radiometer (AMSR-E) instrument, a passive radiance sensor carried aboard NASA's Aqua spacecraft, NOAA's Advanced Very High Resolution Radiometer, NOAA GOES Imager, and NASA's Moderate Resolution Imaging Spectrometer (MODIS) SST data set. Those satellites measure the SST twice a day, but the exact time of the measurement is obscured after the merging process.

Sea Surface Height (SSH) anomaly observations are obtained from the dataset produced by Ssalto/Duacs and distributed by AVISO. Because of errors impicit in estimating the absolute sea level, only the anomalous part of the AVISO SSH product is used in the assimilation. The along-track SSH anomaly data are added to the mapped temporal mean dynamic topography from the model. Then, the spatial mean of the observation is set to be the same as the model spatial mean.

2.3 Pre-processing of observations

If the observations have features whose spatial scales that are smaller than the model can represent, they have no use in a data assimilation experiment. Hence, all observations inside of a model grid cell are averaged if they occur in the same time period. This "super observations" process effectively smooths the highly resolved satellite data to the coarser resolution used in the model.

2.4 Observational error estimates

The minimum of the estimated observational error in SST is set to be 0.01 °C. Except for the Argo floats that have their own error estimation, the observational errors for T

ACPD
12, 20901–20930, 2012

are set to be the same as the SST data. The observational errors for S are also one-quarter of the size of the model standard deviation, but the minimum value is set as 0.01 psu. The observational error of SLH is set to be 1cm.

3 Model and data assimilation procedure

The Regional Ocean Modeling System (ROMS) (Moore et al., 2010; Haidvogel et al., 2008; Shchepetkin and McWilliams, 2005) was configured in a domain to include all the cruise tracks from VOCALS-REx, with additional room outside the intensively sampled region to avoid strong influences of the boundary conditions during the fits. The model domain covers 13° S to 27° S and 67° W to 90° W with an approximately 7 km grid interval, and corresponding smoothed topography (Fig. 2). The grid has 32 terrain-following vertical levels that are concentrated more at the surface and ocean bottom. Lateral boundary conditions are taken from the ROMS simulation of Combes et al. (2012). Surface boundary conditions were taken from QuikSCAT wind stresses and from ECMWF Reanalysis Interim air-sea flux data using bulk formulation (Fairall et al., 2003). Initial long-term tests of the model domain without assimilation and forced with regional winds reveals a strong Peru-Humbodlt Current system and a vigorous mesoscale eddy field, indicating the suitability of ROMS in this framework.

The incremental strong constraints four-dimensional variational data assimilation (IS4DVAR) system developed by (Moore et al., 2011) for ROMS was used to estimate the ocean states from observations. The ROMS 4DVAR procedure adjusts the initial condition and surface forcing, within the given error bars, to bring the model fit into a closer correspondence to the observed data, in a least-square sense, over a defined assimilation time window. This strategy uses the tangent linear and adjoint models (Moore et al., 2010) in an iterative inner loop to deal with the non-linearities of the system. After a first-guess non-linear run of ROMS, several purely linear inner loops are executed to reduce the misfit, as measured by the cost function. Then, a non-linear run

ACPD
12, 20901–20930, 2012

is executed again to determine if the misfit is lower than the initial guess. The procedure is then repeated until a satisfactory fit to the observation is achieved.

Since the subsurface data was so limited in space, we used an ad hoc procedure to determine the first-guess model state. We collapsed all the observations onto the same time stamp and executed a IS4DVAR fit of a one-day run of the model to that "date" from a random initial state. This is tantamount to using an optimal interpolation of all the data as a first-guess initial condition for the assimilation procedure.

We first attempted to fit the entire 30 days of the REx cruises, but non-linearities in the system did not admit convergence to a state that resembled the observations. We then broke the REx survey into two 15-day periods, 1–15 November (Fit-1) and 16–30 November (Fit-2), and these converged to realistic representations of the ocean flows. In our case, we used fifteen inner loops and three outer (non-linear) loops before arriving at the final state estimate.

4 Model fitting results

Figure 3 shows the reduction of the normalized absolute error (NAE) for the total assimilation period. If the NAE is one, it means the misfit between the observation and the interpolated model states is the same as the observational error. In November 2008, the mean NAE became roughly one after the ROMS 4DVAR procedure decreased the normalized misfit by 70 % on average. In general, the reductions of the NAE are greater when the initial errors are larger. The SST has the biggest NAE both before and after the assimilation for the first 15 days and the SSH has the biggest error in the second 15 days. NAEs for other variables are reduced to approximately the observational error level.

Taylor diagrams (Taylor, 2001) offer a visual way to compare the performances of several models with respect to the observations by showing their standard deviation, correlation, and the centered root-mean-square (RMS) difference. Figure 4 shows the changes in normalized statistics for SSH, T and S on the Taylor diagrams for each fit.

ACPD
12, 20901–20930, 2012

The arrows indicate the changes in normalized statistics after data assimilation with the start of the arrow indicating the initial model state and the end of the arrowhead at the location of the final model state after assimilation. The data assimilation improved the statistics for all variables in both time periods.

The model fits to subsurface profiles from the CTD casts are shown in Figs. 5 and 6 for the first and second fortnights of November. The fits for both periods show a reduction in the model-data misfits by a large fraction in the upper 200 m of the profiles where the misfits are the largest. The middle bottom panel in the figures show the horizontal location of the profiles. The eddy at 76° W and 19.5° S was mainly surveyed in the first fortnight but was also profile some more in the second fortnight.

The model fits of SSH anomaly are shown in Fig. 7 compared with those estimated from AVISO. Both fits reveal similar large-scale patterns as the observations, with finer-scale structures in the model due to its higher resolution. The intensively surveyed eddy at 76° W and 19.5° S has a low SSH signature evident in both observations and model. The currents from the model plotted as vectors also reveal a cyclonic eddy at this location and much finer scale structures around it.

The model fits of SST along with satellite observations are shown in Fig. 8. Both fits reveal similar large-scale patterns similar to the observations, with considerable mesoscale structures that qualitatively resemble the observations. These mesoscale structures are not well constrained by the fit, likely due to the lack of adequate sub-surface observations away from the cruise tracks, as well as nonlinearities in their evolution.

Subsurface variability is shown in Fig. 9, in which the 250 m temperature and velocity fields is shown for three times during November. The subsurface expression of the eddy at (76° W, 19.5° S) is clearly captured by the fits. The 250 m temperature shows the doming of the isotherms beneath the cyclonic eddy as found in previous studies of eddy structure in this region (Chaigneau et al., 2011; Holte et al., 2012). During the VOCALS campaign, it migrates slightly northwestward and elongates in the northwest-southeast orientation, possibly indicative of an eddy splitting event.

ACPD
12, 20901–20930, 2012

The strength of nonlinearities in this flow is tested with the Okubo-Weiss (OW) parameter (Weiss, 1991; Okubo, 1970) (Fig. 9d), which describes the relative dominance of strain and vorticity. A threshold for OW must be set so as to distinguish coherent structures from the background field. Previous studies with satellite altimetry data have used $OW = 0.2\ \sigma_{OW}$, where σ_{OW} is the spatial standard deviation of OW. In an elliptic regime, rotation dominates deformation (and vice versa for hyperbolic). Eddy cores can therefore be identified as connected regions with negative values of OW. This criterion for eddy identification has been used successfully with data from sea level altimetry maps (Isern-Fontanet et al., 2003; Morrow et al., 2004). Closed contour structures with length scales greater than 10–20 km in Figure 7d are indicative of eddy-like structures (Chelton et al., 2007). The OW highlights the eddy at (76° W, 19.5° S) as well as the two cyclonic eddies at 80° W and 84° W.

Figure 10 shows eddy kinetic energy averaged for a week during the cruise period when the subsurface eddy at (76° W, 19.5° S) was intensively surveyed. The top panel (Fig. 10a) shows the overlaying SLA contours from satellite altimetry and the second panel (Fig. 10b) shows the contours of model SLA overlaid on EKE. This further reveals the intensity of the eddies (cyclonic and anticyclonic) showing that the observed eddy was of moderate intensity compared to the other eddies that occurred during this time period. The bottom two panels (Fig. 10c and Fig. 10d) show the evolution of the EKE over a period of a week during the cruise period revealing persistent eddy structures which morph into different shapes preserving their EKE as they propagate.

The vertical structure of the eddy field is shown in a depth-longitude cross-section in Fig. 11. The deep structure of the eddy at 76° W is evident by the doming isopycnals extending from 50 m to 400 m depth. The subsurface velocities associated with this are stronger near the surface, reaching 40 cm s^{-1}, and weaker at depth, typically 10–20 cm s^{-1}. The core of the eddy has a salinity minimum, as shown in Fig. 12, where the velocity field has its zero crossing, which indicates its circulation strength and its isolation from the surrounding waters. This is consistent with the similar cyclonic eddies with salinity minima studied previously by Echevin et al. (2004). They show during

ACPD
12, 20901–20930, 2012

spring, several lower salinity lenses are evidenced at 100 m depth during the period from 2000–2004. These salinity lenses which have been related to the Eastern South Pacific Intermediate Water in previous studies (Schneider et al., 2003), seem to be relatively isolated and poorly mixed with surrounding waters especially near the Nazca ridge, a topographic feature which stretches diagonally across the domain (Fig. 2). This ridge is also a region of high nonlinear eddy activity as evidenced in the Figure 9d of higher number of closed contours of OW parameter in this region during this period. This topographic feature can influence the vertical structure of the eddies in this region and concomitant trapping of salinity cores from the eddies.

5 Upper ocean heat budget

In this section, a regional heat balance is constructed for the upper ocean of the high resolution ocean state estimate for a two week period. The time-mean oceanic heat balance integrated over the upper ocean is

$$\int_{z_0}^{\eta} \rho_0 C_p \partial_t \overline{T}\, dz = -\int_{z_0}^{\eta} \rho_0 C_p \nabla \cdot \overline{\boldsymbol{u}T}\, dz + Q_{\text{net}} - \rho_0 C_p \overline{\kappa_v \partial_z T}|_{z_0} - \int_{z_0}^{\eta} \rho_0 C_p \kappa_h \nabla^2 T, \quad (1)$$

where Q_{net} is the net surface heat flux, C_p is the specific heat of seawater at constant pressure, ρ_0 is the density of seawater, $\boldsymbol{u}$ is the total velocity vector, T is temperature and κ_v and κ_h are the subgrid-scale horizontal and vertical eddy diffusivity parameters. The first term on the left hand side is the rate of temperature change (or temperature tendency), the first term on the right-hand side is the temperature advection followed by the terms for net surface heat flux and horizontal and vertical diffusion, respectively. These terms are saved and averaged over the duration of the ROMS simulation.

Although a long-term balance of the heat equation can not be computed with this short data assimilation fit, the ocean state estimate can still be analyzed to understand the key mechanisms which are in balance during the period of the cruise. The solution

ACPD
12, 20901–20930, 2012

is integrated from 0m to 400 m depth, below which vertical advection is small, based on inspecting plots of this field. Hence, the vertically integrated advection term in the heat balance equation is dominantly the horizontal advection term.

The spatial pattern of each term of Eq. (1) in the model heat balance for the period during which the eddy was observed intensively is shown in Fig. 13. The advection (Fig. 13b) and vertical diffusion (Fig. 13c) terms are the dominant terms, with magnitudes similar to that of the temperature tendency for this short-term two-week-averaged balance. The horizontal diffusion term (Fig. 13d) has a smaller magnitude and has much smaller spatial scale structures than the other terms, and will be ignored in subsequent discussion.

The pattern of the mean sea level anomaly during the period is plotted as line contours over the tendency (color) contours in Fig. 13a. The cyclonic eddy at 76° W exhibits a dipolar pattern in the heat budget with advection by cooling on the western side and vice versa to the east. The pattern is nearly symmetric, with cooling and warming, averaging nearly to zero over the spatial pattern of the eddy. Likewise, box averages over larger areas of the the cruise region yield very small imbalances for the advection term. The vertical diffusion term, in contrast, (Fig. 13c) has a net cooling effect over the entire domain. This term includes the net warming at the surface as well as the cooling by vertical mixing throughout the water column. Clearly the vertical mixing processes contribute significantly to cooling broad-scale averages of the upper ocean in this region and dominates over the lateral advection effects of the smaller-scale eddies.

The cumulative long-term impact of these eddies on the heat budget cannot be identified in these short data assimilation fits. Previous work by Colbo and Weller (2007) suggest that the divergence of the eddy heat flux, horizontal advection and the horizontal and vertical diffusion terms are all significant and important in the mean heat balance. In contrast, modeling studies by (Toniazzo et al., 2009; Zheng et al., 2010) revealed that the eddy heat flux divergence is not spatially coherent on the large scale, so the effect of eddies do not significantly impact the heat budget in the southeast Pacific when averaged over a large region. This latter interpretation is consistent with the

ACPD
12, 20901–20930, 2012

results presented here, as well as with the observational study by (Holte et al., 2012). Holte et al. (2012) show that cyclonic and anticyclonic eddies in the Southeast Pacific are observed to occur with similar frequency and have opposite effects on the surface layer temperature. Due to this symmetry, they conclude, consistent with the results presented in this section, that the eddy heat flux divergence is likely to be negligible in the upper ocean heat budget in this region.

6 Summary and discussion

This study examines the upper-ocean variability observed during the VOCALS-REx cruise of 2008 by using ocean state estimation with ROMS. Nonlinearities in the system prevent a 30-day fit, so two 15-day fits are executed for the available observations of hydrographic temperature and salinity and satellite fields of SST and sea-level height. The fits reduce the cost function significantly and ROMS is able to successfully reproduce both large-scale smaller-scale features of the flows observed during the cruises.

Particular attention is focused on an intensively studied eddy at 76° W, 19° S. The ROMS fits capture this eddy as an isolated rotating vortex with a strong subsurface signature in velocity, temperature and anomalous low salinity. The eddy has an average temperature anomaly of approximately −0.5 °C over a depth range from 50–600 m and features a cold anomaly of approximately −1 °C near 150 m depth. The eddy moves northwestward and elongates during the second 15-day fit. It exhibits a strong signature in the OW parameters, which indicates significant nonlinearity in its evolution.

The heat balance for the period of the cruise from the ocean state estimate reveals that the horizontal advection and the vertical mixing processes are the dominant terms that balance the temperature tendency of the upper layer of the ocean locally in time and space. Areal averages, however, around the eddies or around the cruise tracks suggest that vertical mixing processes generally balance the surface heating. There is a lack of consensus regarding the importance of eddy heat flux divergence in balancing the upper ocean heat budget for this region in studies over the past decade Colbo

ACPD
12, 20901–20930, 2012

and Weller (2007); Toniazzo et al. (2009); Zheng et al. (2010); Holte et al. (2012). The results presented here are in agreement with modeling studies by Toniazzo et al. (2009); Zheng et al. (2010) and observational studies by Holte et al. (2012) indicating that over a large area in the SEP region, the average eddy heat flux divergence is not significant compared to the vertical diffusion in maintaining the cool SSTs in this region. This contradicts other observational studies by Colbo and Weller (2007) and modeling studies by Colas et al. (2011) who conclude that eddies do play a significant role in the upper ocean heat balance in this region.

The results in this study may also be of interest to the biogeochemical community to investigate links between ecosystems, biogenic oceanic aerosols and mesoscale eddies in the highly productive Peru-Chile Current System. Further work is needed to understand how the upper-ocean processes couple to the atmospheric processes and the role of the oceanic aerosols and its complex relationship with the stratus deck in modulating and maintaining the temperate climate in this region.

Acknowledgement. This research forms a part of the Ph.D. dissertation of AS. This work was supported by National Science Foundation funding (OCE-0744245) VOCALS: Mesoscale Ocean Dynamical Analysis with Synoptic Data Assimilation and Coupled Ocean-Atmosphere Modeling and (OCE10-26607) for the California Current Ecosystem Long Term Ecological Research site. RAW and FS were supported by NOAA (NA09OAR4320129). We thank the scientific party and the crew of the NOAA ship Ronald H. Brown who helped in collecting the hydrographic data during VOCALS-REx.The altimeter products were produced by SSALTO-DUACS and distributed by AVISO with support from CNES. The AVHRR-Pathfinder SST data were obtained from the Physical Oceanography Distributed Active Archive Center (PO.DAAC) at the NASA Jet Propulsion Laboratory. AS would like to thank Dian Putrasahan, Jamie Holte, Vincent Combes for many discussions regarding the ocean-atmosphere dynamics in this region.

ACPD
12, 20901–20930, 2012

References

Albert, A., Echevin, V., Lévy, M., and Aumont, O.: Impact of nearshore wind stress curl on coastal circulation and primary productivity in the Peru upwelling system, J. Geophys. Res., 115, C12033, doi:10.1029/2010JC006569, 2010. 20904

Amador, J., Alfaro, E., Lizano, O., and Magaña, V.: Atmospheric forcing of the eastern tropical Pacific: A review, Prog. Oceanogr., 69, 101–142, doi:10.1016/j.pocean.2006.03.007, 2006. 20903

Capet, X., Colas, F., Penven, P., Marchesiello, P., and McWilliams, J.: Eddies in eastern boundary subtropical upwelling systems, Ocean modeling in an Eddying regime, Geophys. Monogr. Ser., AGU, Washington DC, 177, doi:10.1029/177GM10, 2008. 20903

Chaigneau, A., Le Texier, M., Eldin, G., Grados, C., and Pizarro, Ó.: Vertical structure of mesoscale eddies in the eastern South Pacific Ocean: A composite analysis from altimetry and Argo profiling floats, J. Geophys. Res., 116, C11025, doi:10.1029/2011JC007134, 2011. 20908

Chelton, D. B., Gaube, P., Schlax, M. G., Early, J. J., and Samelson, R. M.: The Influence of Nonlinear Mesoscale Eddies on Near-Surface Oceanic Chlorophyll, Science, 334, 328–332, doi:10.1126/science.1208897, 2011. 20903

Chelton, D. B., M. Schlax, R. M. Samelson, and R. de Szoeke: Global observations of large oceanic eddies, Geophys. Res. Lett., 34, L15606, doi:10.1029/2007GL030812, 2007. 20909

Clarke, A. D.: Particle Nucleation in the Tropical Boundary Layer and Its Coupling to Marine Sulfur Sources, Science, 282, doi:10.1126/science.282.5386.89, 1998. 20904

Colas, F., J. C. Mcwilliams, X. Capet, and J. Kurian: Heat balance and eddies in the Peru-Chile current system, Clim. Dynam., 39, 509–529, doi:10.1007/s00382-011-1170-6, 2011. 20903, 20913

Colbo, K. and R. Weller: The variability and heat budget of the upper ocean under the Chile-Peru stratus, J. Marine Res., 65, 2007. 20911, 20912, 20913

Combes, V., et al.: Modeling interannual and decadal variability in the Humboldt current upwelling system, J. Phys. Oceanogr., sub judice, 2012. 20906

de Szoeke, S., C. Fairall, D. Wolfe, L. Bariteau, and P. Zuidema: Surface flux observations on the southeastern tropical Pacific Ocean and attribution of SST errors in coupled ocean-atmosphere models. J. Climate, 23, 4152–4174, doi:10.1175/2010JCLI3411.1, 2010. 20903

ACPD
12, 20901–20930, 2012

Echevin, V., I. Puillat, C. Grados, and B. Dewitte: Seasonal and mesoscale variability in the Peru upwelling system from in situ data during the years 2000 to 2004, Gayana (Concepción), 68, 2004. 20909

Fairall, C. W., E. Bradley, J. Hare, A. Grachev, and J. Edson: Bulk parameterization of air–sea fluxes: Updates and verification for the COARE algorithm, J. Climate, 16, doi:10.1175/1520-0442(2003)016<0571:BPOASF>2.0.CO;2, 2003. 20906

Garreaud, R. and R. Muñoz: The low-level jet off the west coast of subtropical South America: Structure and variability, Mon. Weather Rev., 133, doi:10.1175/MWR3074.1, 2005. 20903

Haidvogel, D., et al.: Ocean forecasting in terrain-following coordinates: Formulation and skill assessment of the Regional Ocean Modeling System, J. Comput. Phys., 227, doi:10.1016/j.jcp.2007.06.016, 2008. 20906

Hind, A. J., Rauschenberg, C. D., Johnson, J. E., Yang, M., and Matrai, P. A.: The use of algorithms to predict surface seawater dimethyl sulphide concentrations in the SE Pacific, a region of steep gradients in primary productivity, biomass and mixed layer depth, Biogeosciences, 8, 1–16, doi:10.5194/bg-8-1-2011, 2011. 20903

Holte, J., F. Straneo, C. Moffat, B. Weller, and T. Farrar: Structure, properties, and heat content of eddies in the southeast Pacific Ocean. J. Phys. Oceanogr., sub judice, 2012. 20904, 20908, 20912, 20913

Isern-Fontanet, J., García-Ladona, E., and Font, J.: Identification of marine eddies from altimetric maps, Journal of Atmospheric and Ocean. Technol., 20, doi:10.1175/1520-0426(2003)20<772:IOMEFA>2.0.CO;2, 2003. 20909

Klein, S. and D. Hartmann: The seasonal cycle of low stratiform clouds. J. Climate, 6, 1587–1606, doi:10.1175/1520-0442(1993)006<1587:TSCOLS>2.0.CO;2, 1993. 20903

Large, W. G. and G. Danabasoglu: Attribution and Impacts of Upper-Ocean Biases in CCSM3, J. Climate, 19, doi:10.1175/JCLI3740.1, 2006. 20903

Ma, C. C., C. R. Mechoso, A. W. Robertson, and A. Arakawa: Peruvian stratus clouds and the tropical Pacific circulation: A coupled ocean-atmosphere GCM study, J. Climate, 9, doi:10.1175/1520-0442(1996)009<1635:PSCATT>2.0.CO;2, 1996. 20902

Mechoso, C. R., et al.: The seasonal cycle over the tropical Pacific in coupled ocean-atmosphere general circulation models, Mon. Weather Rev., 123, doi:10.1175/1520-0493(1995)123<2825:TSCOTT>2.0.CO;2, 1995. 20902, 20903

Moore, A. M., H. G. Arango, G. Broquet, B. S. Powell, J. Zavala-Garay, and A. Weaver: The Regional Ocean Modeling System (ROMS) 4-Dimensional Variational Data Assimi-

ACPD

12, 20901–20930, 2012

lation Systems: I-System overview and formulation. Progress in Oceanogr., 91, 34–49, doi:10.1016/j.pocean.2011.05.004, 2010. 20906
Moore, A. M., et al.: The Regional Ocean Modeling System (ROMS) 4-dimensional variational data assimilation systems. Part II: Performance and Application to the California Current System, Prog. Oceanogr., 91, 50–73, doi:10.1016/j.pocean.2011.05.003, 2011. 20906
Morrow, R., F. Birol, D. Griffin, and J. Sudre: Divergent pathways of cyclonic and anti-cyclonic ocean eddies, Geophys. Res. Lett., 31, L24311, doi:10.1029/2004GL020974, 2004. 20909
Okubo, A.: Horizontal dispersion of floatable particles in the vicinity of velocity singularities such as convergences, Deep Sea Res. Oceanogr. Abstr., 17, 445–454, doi:10.1016/0011-7471(70)90059-8, 1970. 20909
Penven, P.: Average circulation, seasonal cycle, and mesoscale dynamics of the Peru Current System: A modeling approach, J. Geophys. Res., 110, doi:10.1029/2005JC002945, 2005. 20903
Schneider, W., Fuenzalida, R., Rodríguez-Rubio, E., Garcés-Vargas, J., and Bravo, L.: Characteristics and formation of Eastern South Pacific Intermediate Water, Geophys. Res. Lett., 30, 1581, doi:10.1029/2003GL017086, 2003. 20910
Shchepetkin, A. and McWilliams, J.: The regional oceanic modeling system (ROMS): a split-explicit, free-surface, topography-following-coordinate oceanic model, Ocean Model., 9, 347–404, doi:10.1016/j.ocemod.2004.08.002, 2005. 20906
Taylor, K.: Summarizing multiple aspects of model performance in a single diagram, J. Geophys. Res., 106, 7183–7192, doi:10.1029/2000JD900719, 2001. 20907
Toniazzo, T., Mechoso, C. R., Shaffrey, L. C., and Slingo, J. M.: Upper-ocean heat budget and ocean eddy transport in the south-east Pacific in a high-resolution coupled model, Clim. Dynam., 35, 1309–1329, doi:10.1007/s00382-009-0703-8, 2009. 20911, 20913
Weiss, J.: The dynamics of enstrophy transfer in two-dimensional hydrodynamics, Physica D: Nonlin, Phenom,, 48, 273–294, doi:10.1016/0167-2789(91)90088-Q, 1991. 20909
Wood, R., Mechoso, C. R., Bretherton, C. S., Weller, R. A., Huebert, B., Straneo, F., Albrecht, B. A., Coe, H., Allen, G., Vaughan, G., Daum, P., Fairall, C., Chand, D., Gallardo Klenner, L., Garreaud, R., Grados, C., Covert, D. S., Bates, T. S., Krejci, R., Russell, L. M., de Szoeke, S., Brewer, A., Yuter, S. E., Springston, S. R., Chaigneau, A., Toniazzo, T., Minnis, P., Palikonda, R., Abel, S. J., Brown, W. O. J., Williams, S., Fochesatto, J., Brioude, J., and Bower, K. N.: The VAMOS Ocean-Cloud-Atmosphere-Land Study Regional Experiment (VOCALS-REx):

ACPD
12, 20901–20930, 2012

goals, platforms, and field operations, Atmos. Chem. Phys., 11, 627–654, doi:10.5194/acp-11-627-2011, 2011. 20903, 20904

Xie, S.-P.: The shape of continents, air-sea interaction, and the rising branch of the Hadley circulation. Advances in Global Change Research, Kluwer Academic Publishers, 21, 121–152, doi:10.1007/978-1-4020-2944-8_4, 2004. 20903

Yang, M., Blomquist, B. W., and Huebert, B. J.: Constraining the concentration of the hydroxyl radical in a stratocumulus-topped marine boundary layer from sea-to-air eddy covariance flux measurements of dimethylsulfide, Atmos. Chem. Phys., 9, 9225–9236, doi:10.5194/acp-9-9225-2009, 2009. 20903, 20904

Yang, M., Huebert, B. J., Blomquist, B. W., Howell, S. G., Shank, L. M., McNaughton, C. S., Clarke, A. D., Hawkins, L. N., Russell, L. M., Covert, D. S., Coffman, D. J., Bates, T. S., Quinn, P. K., Zagorac, N., Bandy, A. R., de Szoeke, S. P., Zuidema, P. D., Tucker, S. C., Brewer, W. A., Benedict, K. B., and Collett, J. L.: Atmospheric sulfur cycling in the southeastern Pacific – longitudinal distribution, vertical profile, and diel variability observed during VOCALS-REx, Atmos. Chem. Phys., 11, 5079–5097, doi:10.5194/acp-11-5079-2011, 2011. 20903, 20904

Zheng, X., Albrecht, B., Jonsson, H. H., Khelif, D., Feingold, G., Minnis, P., Ayers, K., Chuang, P., Donaher, S., Rossiter, D., Ghate, V., Ruiz-Plancarte, J., and Sun-Mack, S.: Observations of the boundary layer, cloud, and aerosol variability in the southeast Pacific near-coastal marine stratocumulus during VOCALS-REx, Atmos. Chem. Phys., 11, 9943–9959, doi:10.5194/acp-11-9943-2011, 2011. 20903

Zheng, Y., Shinoda, T., Kiladis, G., Lin, J., and Metzger, E.: Upper Ocean Processes Under the Stratus Cloud Deck in the Southeast Pacific Ocean, J. Phys. Oceanogr., 40, 103–120, doi:10.1175/2009JPO4213.1, 2010. 20903, 20911, 20913

ACPD

12, 20901–20930, 2012

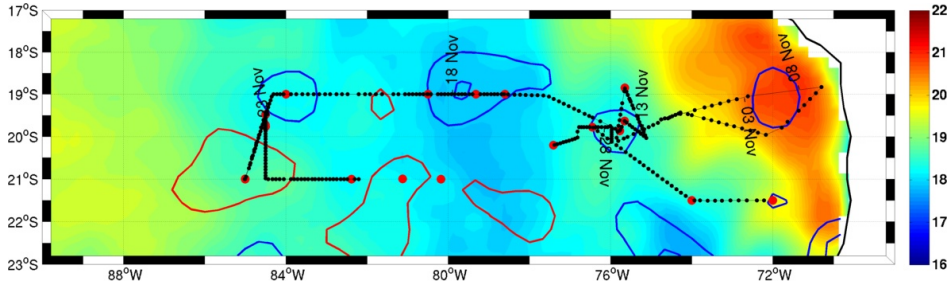

Fig. 1. SST (°C) from AVHRR for 18 November 2008 (color contours) and ±5 cm Sea Level anomaly contours (line contours) from AVISO during VOCALS cruise period. The cyclonic eddies are marked as blue contours and the anticyclonic ones as red. The NOAA ship Ron Brown cruise track from 1 to 30 November 2008 is shown as points where the 438 UCTD (black dots) and CTD(large red dots) casts were taken.

ACPD
12, 20901–20930, 2012

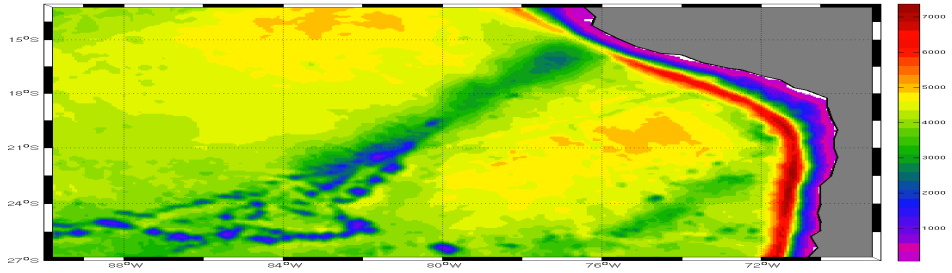

(a) Bathymetry

Fig. 2. Horizontal domain used for the ROMS experiments with the model bathymetry (color) plotted in meters depth. The Nazca ridge cuts across the domain diagonally changing depths on either side from 5000 m to 2000 m.

ACPD
12, 20901–20930, 2012

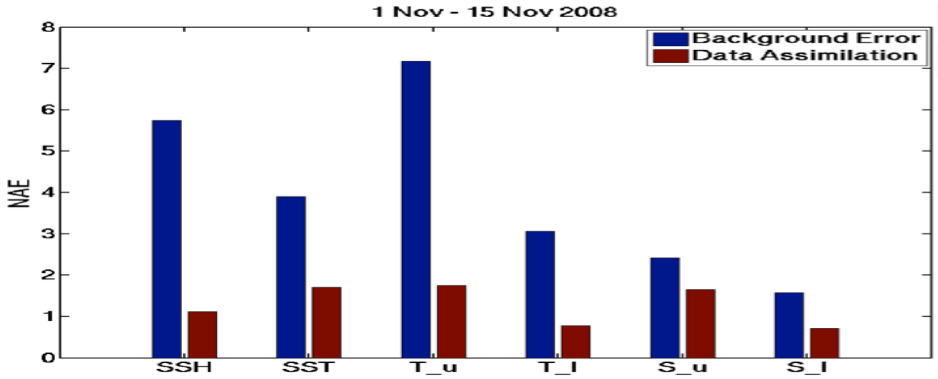

(a) 1–15 November

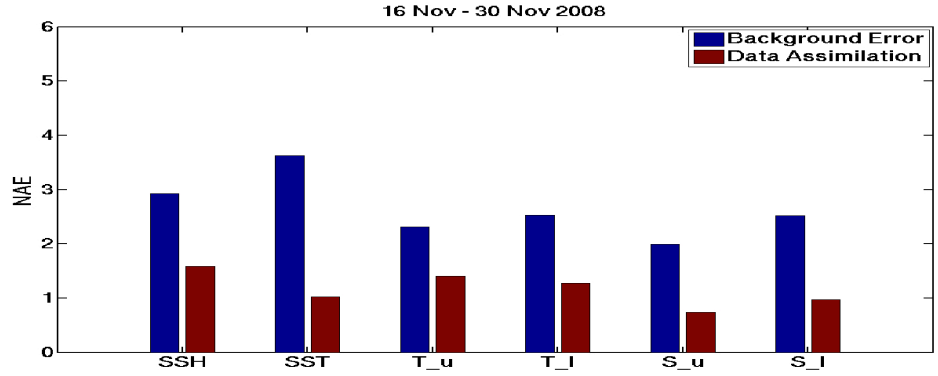

(b) 16–30 November

Fig. 3. Normalized mean absolute error changes for the two 15 day assimilation fits. **(a)** For the first 15 day fit for 1–15 November 2008. **(b)** For the second 15 day fit for 16–30 November 2008 for sea surface height (SSH), sea surface temperature (SST), temperature in upper 100 m (T_u), temperature below 100 m (T_l), salinity in upper 100 m (S_u) and salinity below 100 m (S_l).

ACPD
12, 20901–20930, 2012

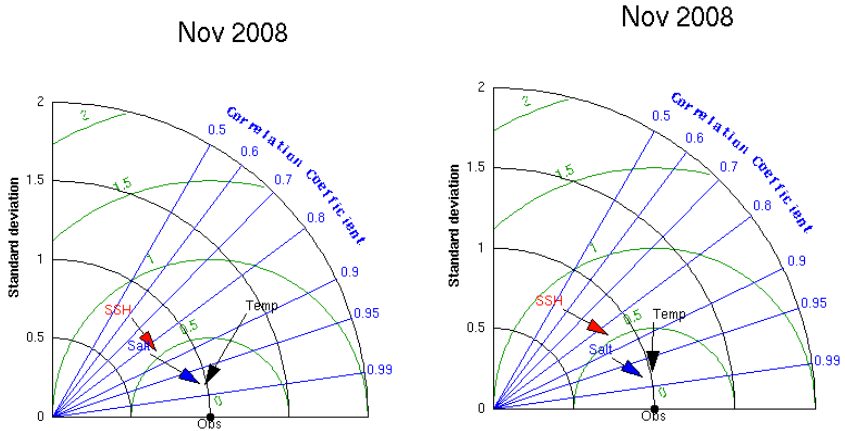

Fig. 4. Taylor Diagram for the two 15 day assimilation fits. **(a)** For the first 15 day fit for 1–15 November 2008. **(b)** For the second 15 day fit for 16–30 November 2008 for salinity (blue arrow), SSH (red arrow) and temperature (black arrow).

ACPD
12, 20901–20930, 2012

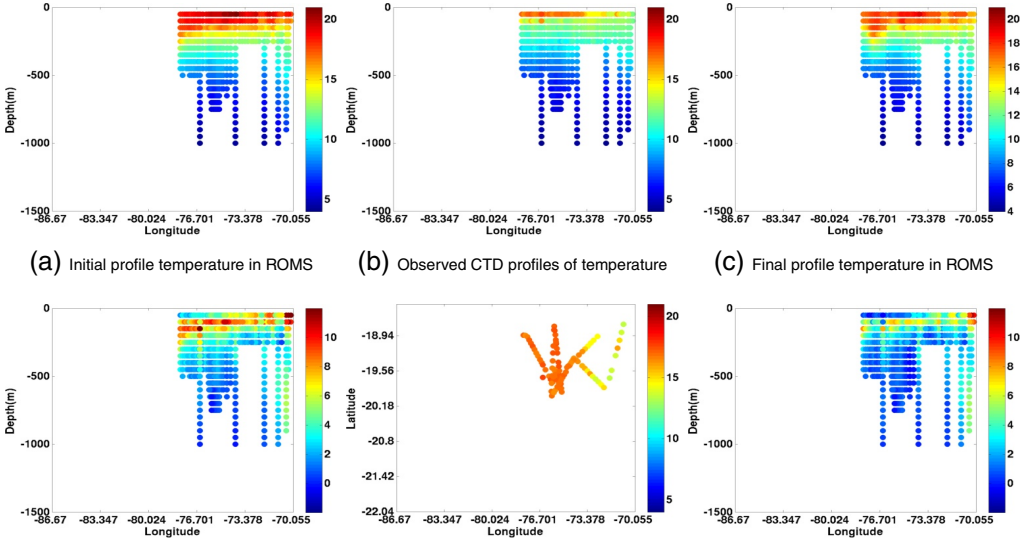

(a) Initial profile temperature in ROMS (b) Observed CTD profiles of temperature (c) Final profile temperature in ROMS

(d) Initial misfit in temperature Profiles in ROMS (e) Horizontal positions of profiles (f) Final misfit in temperature profiles in ROMS

Fig. 5. (a, c) Model and **(b)** observed profile temperature values (in °C) before and after assimilation. The horizontal location of the profiles are shown in **(e)**. The **(d)** initial model misfit before assimilation and **(f)** final model misfit after assimilation for the first 15 day fit from 1 to 15 November 2008.

ACPD
12, 20901–20930, 2012

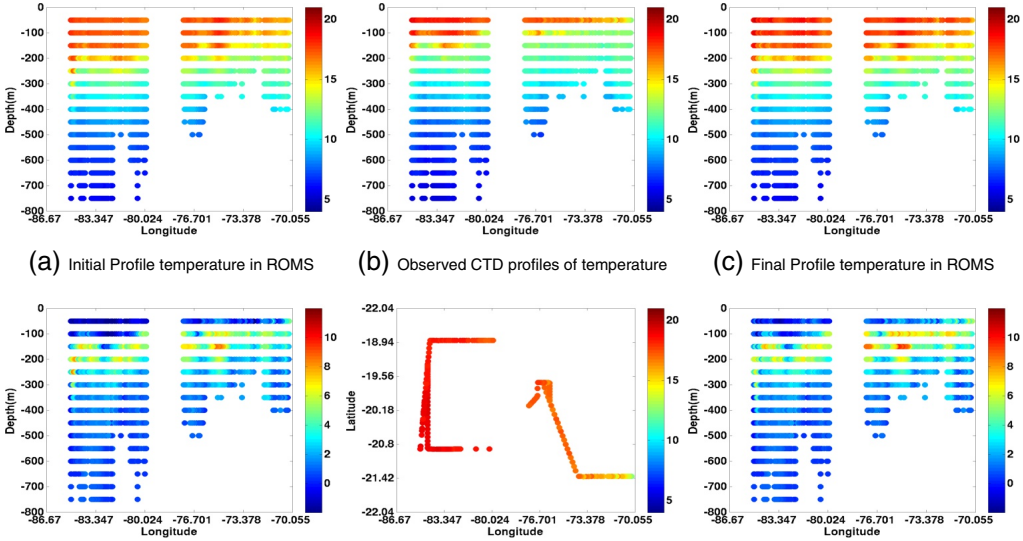

Fig. 6. (a, c) Model and **(b)** observed profile temperature (in ˚C) values before and after assimilation. The horizontal location of the profiles are shown in **(e)**. The **(d)** initial model misfit before assimilation and **(f)** final model misfit after assimilation for the second 15 day fit from 16 to 30 November 2008.

ACPD
12, 20901–20930, 2012

Data assimilative perspective of oceanic mesoscale eddy evolution

A. C. Subramanian et al.

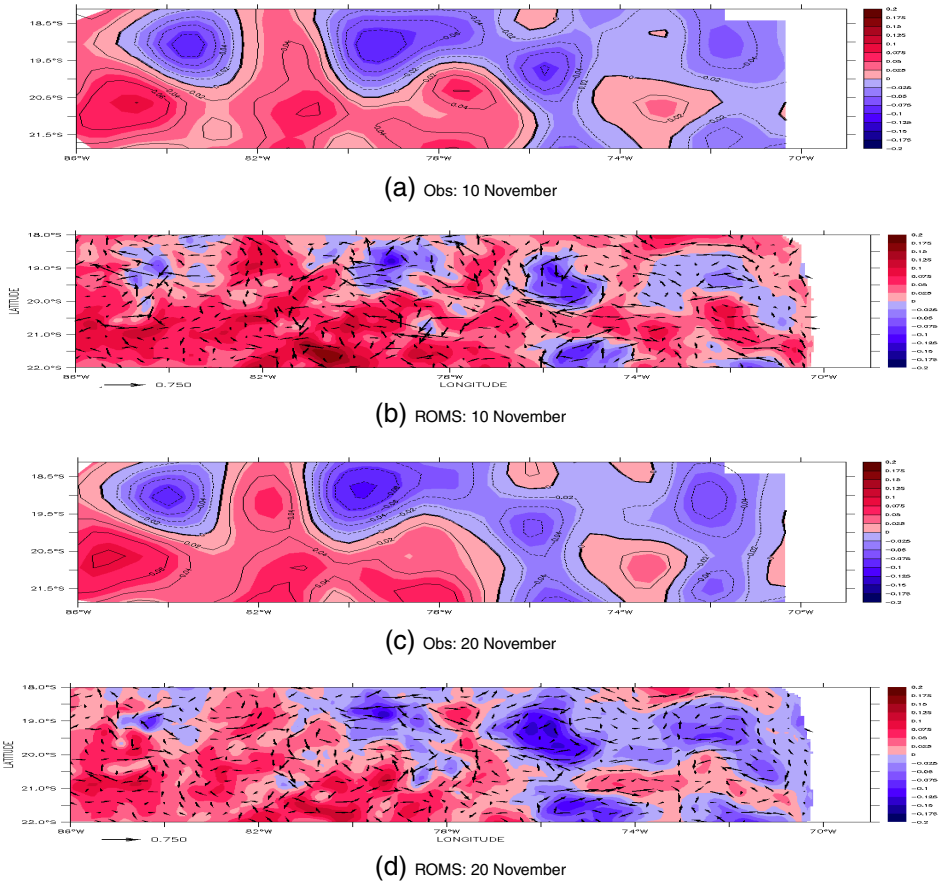

Fig. 7. Sea level anomaly (in meters) from AVISO mapped fields in the **(a)** and **(c)** and from the ROMS ocean state estimate in **(b)** and **(d)**. The velocities from the model are overlaid on the sea level anomaly contours to reveal cyclonic and anticyclonic eddies.

ACPD
12, 20901–20930, 2012

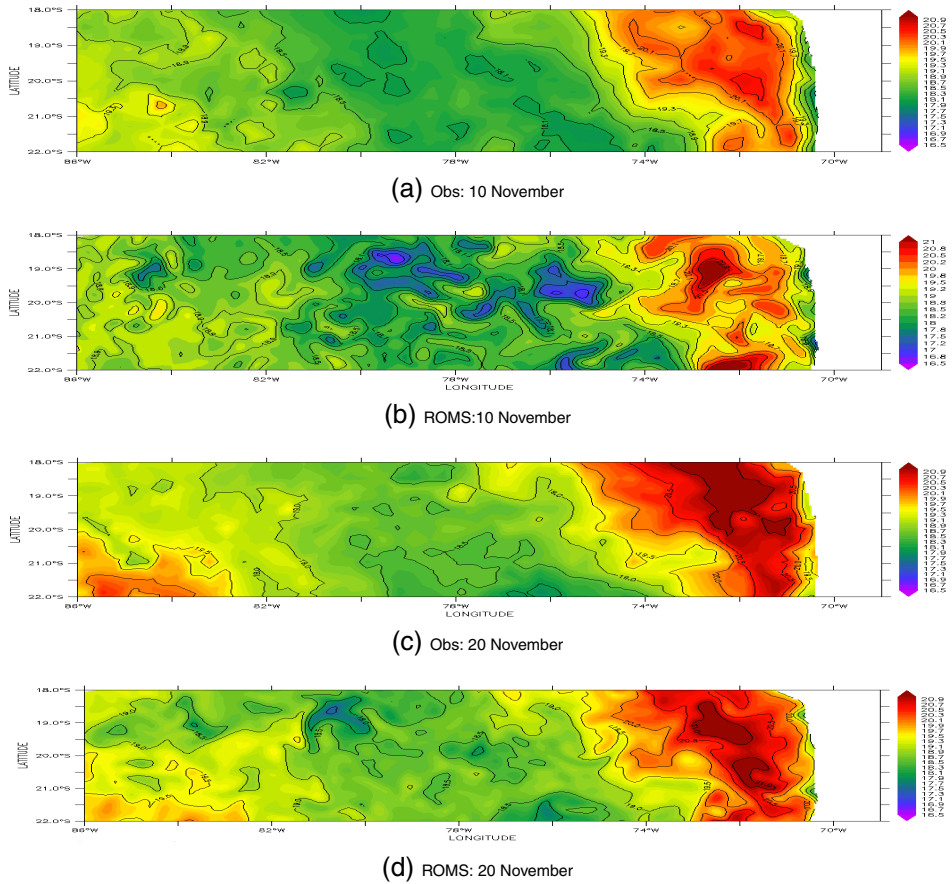

Fig. 8. SST (in ˚C) from NOAA Optimally Interpolated observations in **(a)** and **(c)** and SST from ROMS with the model velocities overlaid for the days 10 and 20 November 2008.

ACPD
12, 20901–20930, 2012

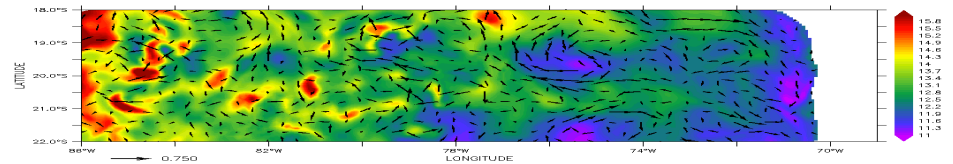

(a) ROMS:10 November

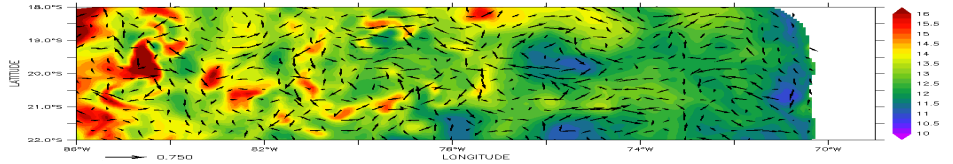

(b) ROMS:14 November

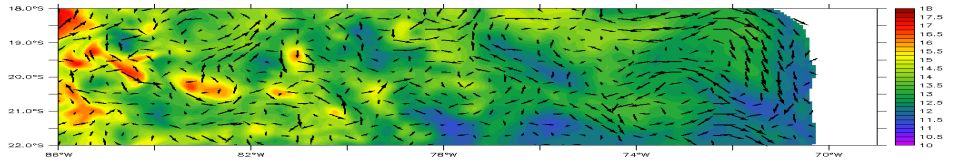

(c) ROMS:20 November

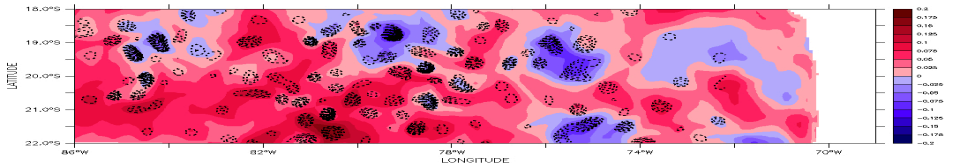

(d) ROMS SSH:10 November

Fig. 9. Temperature (in ˚C) at 250 m Depth in the ocean state estimate for three different days **(a)** 10 November, **(b)** 14 November and **(c)** 20 November showing the evolution of the eddy in time in the model. The last **(d)** is the color contours of SLA with the Okubo-Weiss parameter overlaid on top to show eddy like structures.

ACPD
12, 20901–20930, 2012

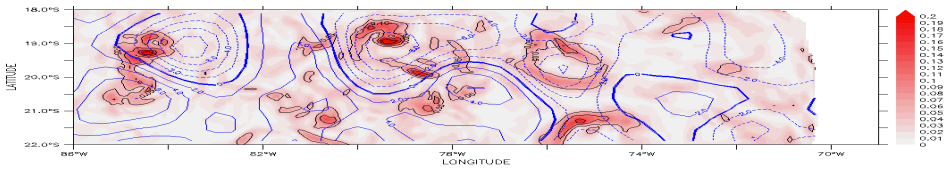

(a) ROMS EKE averaged for 1–15 November with Observed SLA line contours overlaid for 11 November

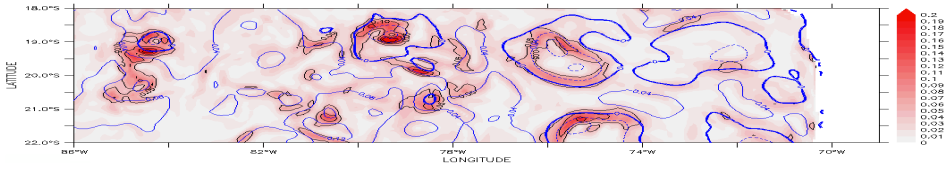

(b) ROMS EKE averaged for 1–15 November with ROMS SLA line contours overlaid for 11 November

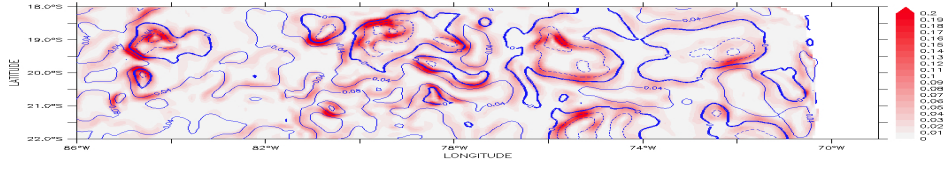

(c) EKE with ROMS SLA Contours for 9 November

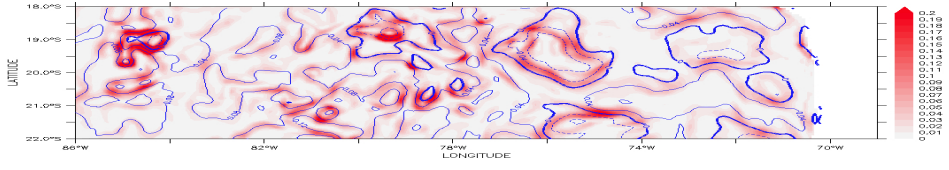

(d) EKE with ROMS SLA Contours for 15 November

Fig. 10. Eddy Kinetic Energy (EKE) averaged for the first two weeks of November from the model overlaid on the **(a)** AVISO SLA and **(b)** ROMS SLA. EKE are daily averaged for **(c)** 9 November and **(d)** 15 November.

ACPD
12, 20901–20930, 2012

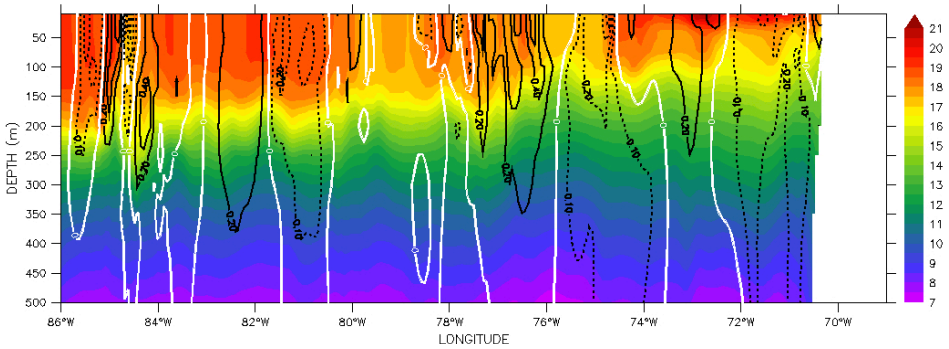

Fig. 11. Vertical temperature (in °C) profiles (color) and meridional velocity (m s^{-1}, line contours) with positive values (continuous lines) and negative values (dashed lines) for 10 November revealing the eddy structure in depth. The profile is plotted at 20° S from 86° W to 69° W

ACPD
12, 20901–20930, 2012

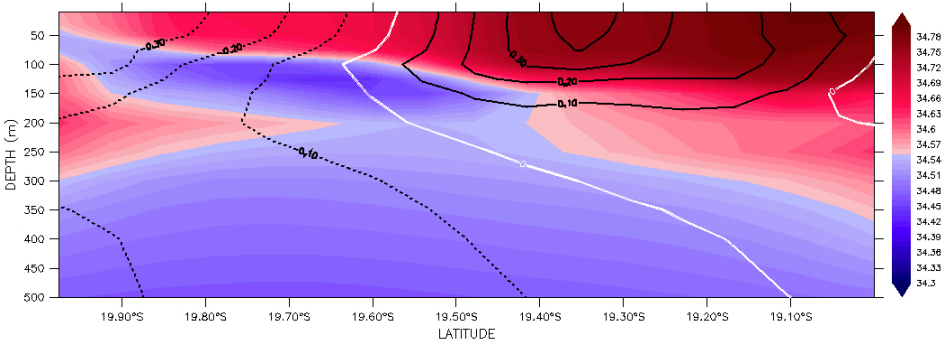

Fig. 12. Zonal velocities ($m\,s^{-1}$) of eddy at 76° W on the same day 10 November with the color contours showing salinity (psu). The positive velocities are shown as continuous lines and the negative values as dashed line contours. The cross-section is from 20° S to 19° S.

ACPD
12, 20901–20930, 2012

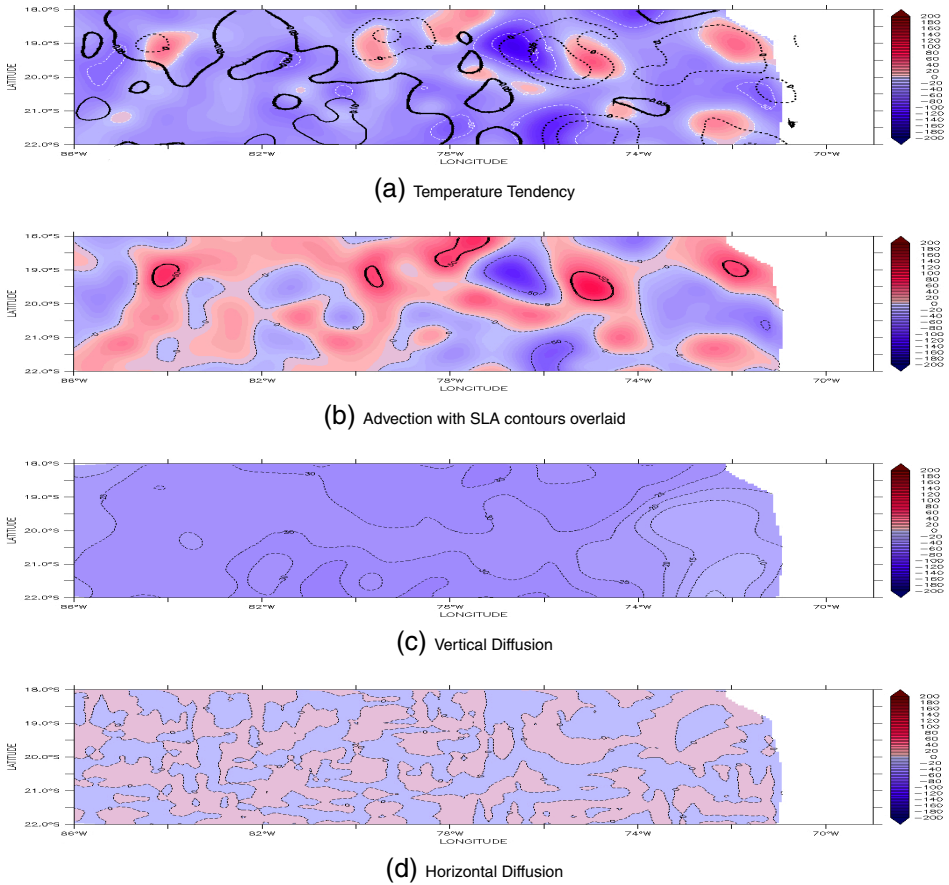

Fig. 13. Spatial maps of heat budget (W m^{-2}) terms from the model for 86° W–69° W and 22° S–18° S. The heat budget terms are integrated to the depth of about 400 m and for a period of two weeks when the eddy was strongest.

ACPD
12, 20901–20930, 2012